Inorganic Chemistry

Article

pubs.acs.org/IC

DFT Study of Uranyl Peroxo Complexes with H_2O, F^-, OH^-, CO_3^{2-}, and NO_3^-

Samuel O. Odoh*,† and Georg Schreckenbach*

Department of Chemistry, University of Manitoba, Winnipeg, Manitoba, Canada R3T 2N2

Supporting Information

ABSTRACT: The structural and electronic properties of monoperoxo and diperoxo uranyl complexes with aquo, fluoride, hydroxo, carbonate, and nitrate ligands have been studied using scalar relativistic density functional theory (DFT). Only the complexes in which the peroxo ligands are coordinated to the uranyl moiety in a bidentate mode were considered. The calculated binding energies confirm that the affinity of the peroxo ligand for the uranyl group far exceeds that of the F^-, OH^-, CO_3^{2-}, NO_3^-, and H_2O ligands. The formation of the monoperoxo complexes from $UO_2(H_2O)_5^{2+}$ and HO_2^- were found to be exothermic in solution. In contrast, the formation of the monouranyl-diperoxo, $UO_2(O_2)_2X_2^{4-}$ or $UO_2(O_2)_2X^{4-/3-}$ (where X is any of F^-, OH^-, CO_3^{2-}, or NO_3^-), complexes were all found to be endothermic in aqueous solution. This suggests that the monoperoxo species are the terminal monouranyl peroxo complexes in solution, in agreement with recent experimental work. Overall, we find that the properties of the uranyl-peroxo complexes conform to well-known trends: the coordination of the peroxo ligand weakens the $U-O_{yl}$ bonds, stabilizes the σ(d) orbitals and causes a mixing between the uranyl π- and peroxo σ- and π-orbitals. The weakening of the $U-O_{yl}$ bonds upon peroxide coordination results in uranyl stretching vibrational frequencies that are much lower than those obtained after the coordination of carbonato or hydroxo ligands.

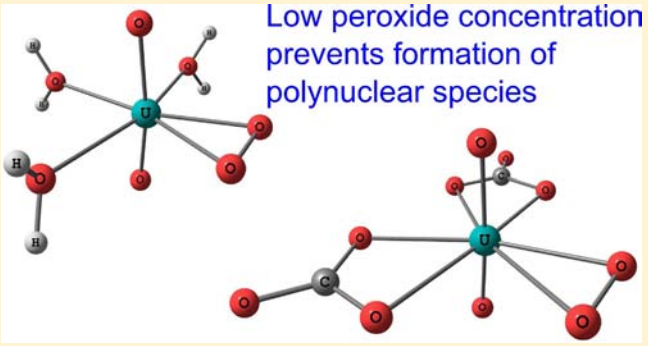

1. INTRODUCTION

The coordination of actinide ions to the peroxide group, O_2^{2-}, has been highlighted for use in nuclear separation technologies due to the crystallization of actinide peroxides complexes,[1] in addition to the intensification of the corrosion of uranium dioxide nuclear fuels after peroxide-induced oxidation.[2,3] The peroxide group has a very strong affinity for uranium resulting in insoluble polynuclear solids at high concentrations and pH.[1,4−7] In fact, studtite, $UO_4{\cdot}4H_2O$, and metastudtite, $UO_4{\cdot}2H_2O$, two hydrated uranyl peroxides, are the only known peroxide containing minerals and are formed from hydrogen peroxide generated by the α-radiolysis of water.[8] Recently, the agglomeration of uranyl-peroxide units into nanoscale cage clusters has been the focus of several studies. Burns et al. have synthesized and characterized a variety of uranyl peroxide hydroxide polyhedral species.[1,4−7,9] These polynuclear clusters mostly adopt a cagelike motif with one of the largest of them being a $[UO_2(OH)(O_2)]_{60}^{60-}$ complex which adopts the buckyball structure of buckminsterfullerene. The reason behind the preference of the cage motif over the linear sheet motif in these and other uranyl-peroxide nanoclusters has been investigated by several workers using electronic structure calculations.[10,11] In their calculations Vlaisavljevich et al. showed that the uranyl-peroxide-uranyl motif found in these clusters is inherently bent as a result of the covalent interaction across the $U-O_2$ bond.[11] They also demonstrated the effect of the size and electronegativity of the counterion on the dihedral $U-O_2-U$ angle.

It is however the case that the solution chemistry of uranyl peroxide has not been investigated to the same extent as its solid-state complexes. The solution chemistry of these peroxide complexes is particularly important in view of the environmental importance of migrating nuclear waste streams. Goff et al.[12] have shown that minute amounts of peroxide can be used to displace a carbonate group from aqueous solutions of $UO_2(CO_3)_3^{4-}$. Structural and spectroscopic characterization of the peroxo-carbonato complex formed revealed it to be $UO_2(O_2)(CO_3)_2^{4-}$ in the form of $K_4[UO_2(O_2)(CO_3)_2]{\cdot}H_2O$. The spectroscopic investigations of Meca et al. have also indicated the existence of two uranyl peroxide-hydroxide complexes at pH 12 in the absence of carbonate species.[13] These species were suggested to be $UO_2(O_2)(OH)_2^{2-}$ and $UO_2(O_2)_2(OH)_2^{4-}$, with the latter, as expected, being more predominant at higher peroxide concentrations. More recently, Zanonato et al. examined the ternary peroxide-hydroxide system in a tetramethylammonium nitrate medium.[14] They found $UO_2(O_2)(OH)^-$ to be the dominant complex from pH 9.5 to 11.5 even though significant amounts of the binuclear complex, $(UO_2)_2(O_2)_2(OH)^-$, was present at around pH 10.5.

Received: March 16, 2013
Published: April 10, 2013

   dx.doi.org/10.1021/ic400652b | *Inorg. Chem.* 2013, 52, 5590−5602

These studies suggest that the uranyl peroxide moiety, $UO_2(O_2)$, could indeed form complexes with a wide variety of ligands insofar as the U(VI) and O_2^{2-} concentration is controlled, to prevent the complexity and precipitation engendered by polynuclear species. Nyman et al. have also recently reported the synthesis of two lithium salts of $UO_2(O_2)_3^{4-}$.[15] They suggested that these monomeric triperoxo systems could play a role in aqueous behavior, redissolution, and self-assembly characteristics of uranyl polynuclear peroxides.

The recent progress being made in the solvent phase and monomer chemistry of uranyl-peroxide species has motivated us to carry out a systematic computational study of the structural and electronic properties of the possible ternary uranyl peroxide complexes with the fluoride, aquo, hydroxo, carbonate, and nitrate ligands. Additionally, we have focused on the characteristic vibrational frequencies of these peroxo complexes, the relative stabilities of their various structures, as well as the trends in their calculated structural properties. Ultimately, the aim of the current work is to provide calculated structural data for the uranyl peroxo complexes. This will hopefully allow for an easier characterization of some these complexes should they be synthesized in the future. All the calculations in this work have been carried out using scalar relativistic density functional theory (DFT). The use of DFT calculations as a complement to the available experimental stoichiometric and structural data of actinide complexes and in predicting the structures of as yet to be synthesized actinide species is well established.[11,16−41]

2. COMPUTATIONAL DETAILS

The geometry optimizations in this work were all carried out with the Gaussian 03 code.[42] Vibrational frequency analyses with the harmonic approximation were carried out after the geometry optimizations to characterize the local minima nature of the optimized structures on the potential energy surfaces. Most of the geometry optimizations and vibrational frequency calculations were carried out in aqueous solution while employing the polarizable continuum solvation (PCM) model.[43] In some cases, the gas phase structures of the complexes were also optimized and presented in this work, for comparison. In the PCM calculations, the default atomic radii of the united force field (UFF) in Gaussian 03 were employed. The peroxide complexes studied in this work were all found to be singlet species. The restricted singlet wave functions are stable with respect to conversion to unrestricted determinants and relaxation of the orbital symmetries. In all the calculations, only complexes with bidentate coordination between the uranium atoms and the peroxo group were considered. Ultrafine grids were used in the numerical integration of the exchange-correlation portion of the density functional. Regarding basis sets, the Stuttgart small-core scalar-relativistic pseudopotential was used to describe the uranium atoms.[44−46] The pseudopotential represents 60 core electrons in uranium while the remaining 32 electrons were represented by the associated valence basis set. The design and use of this pseudopotential−basis set combination reduces the computational expense and allows a wise inclusion of scalar-relativistic effects. To further improve computational efficiency, all g-type functions were removed from the valence basis set. The 6-31+G* basis was used to describe oxygen, nitrogen, fluorine, and carbon atoms while hydrogen atoms were described with the 6-31G basis. We label this scheme in which the uranium RECP and the 6-31+G*/6-31G bases for the nonactinide atoms were employed as B1. The B3LYP[47−49] functional was employed in all the calculations carried out in this current work. Overall the B3LYP/B1 abbreviation is used to describe the functional and basis set combination employed in the calculations.

Single point calculations on the geometries optimized at the B3LYP/B1 level were carried out with a four-component scalar relativistic approach as implemented in the Priroda program.[50] These calculations allowed us to obtain the population based Mayer bond orders which are in our experience good reflections of the formal bond order.[34,37] A basis of double-ζ quality (cc-pVDZ) was used for all the elements for the large component with the corresponding kinetically balanced basis sets for the small component.[51] The B3LYP functional was also employed in the Priroda calculations. This combination of functional and basis set is labeled as B3LYP/B2.

3. RESULTS AND DISCUSSIONS

UO_2^{2+} and Its Peroxo Derivatives. The electronic structure of UO_2^{2+} as well as those of its neptunium and plutonium analogues has been studied extensively.[52−57] At the B3LYP/B1 level and in aqueous solution, the valence region of this dication consists of the σ(f), π(f), σ(d), and π(d) orbitals at −11.1, −11.9, −12.2, and −12.2 eV, respectively. The optimized geometries for UO_2^{2+} and its peroxide derivatives, $UO_2(O_2)_n^{2-n}$, obtained with the PCM solvation model, are shown in Figure 1. For the uranyl peroxide species, $UO_2(O_2)$, $UO_2(O_2)_2^{2-}$, and $UO_2(O_2)_3^{4-}$, the σ and π bonding orbitals of the peroxo ligand are found below the uranyl σ(d) and π(d) orbitals, Table 1. Several valence orbitals of $UO_2(O_2)$ are shown in Figure 2. The U−O_{peroxo} interaction between the uranyl and peroxo units are however found above the uranyl σ(f) orbitals. Here the peroxo lone pair orbitals overlap with uranyl 5f basis functions representing some form of covalent interaction between the uranyl and peroxo units (orbital 31 of Figure 2). The coordination of the second and third peroxide ligands stabilizes the actinyl π(f) orbitals such that there is significant $\sigma(O_2)$−π(f) as well as $\pi(O_2)$−π(d) mixing in the diperoxo and triperoxo complexes, Table 1. In addition to these, the uranyl π(f) orbitals are stabilized below the π(d) orbitals in $UO_2(O_2)_3^{4-}$. The nature of the $\pi(O_2)$−π(d) mixing is reminiscent of the π(d)−μ_3O_2(2p) orbitals that were recently reported in trimeric $[(AnO_2)_3(O)(OH)_3]^+$ complexes of uranium and plutonium.[58] In that study, the degree of stability conferred by the central μ_3-oxo ligand on the hexagonal trimer shape was found to be greater for the uranium complex and lower for the plutonium complex. A similar difference in the mixing of the $\sigma(O_2)$ and $\pi(O_2)$ orbitals with the uranyl and plutonyl π(f) and π(d) orbitals might also exist for the peroxide complexes. This means that one would expect the uranyl

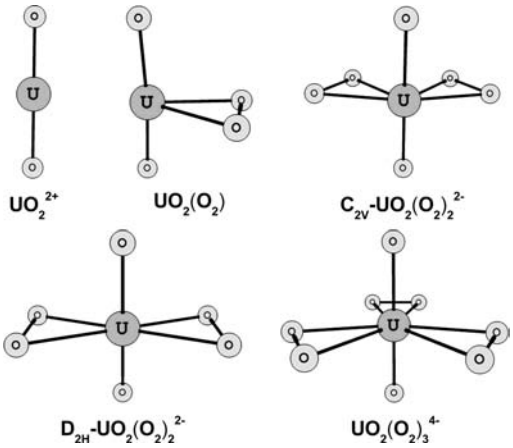

Figure 1. Structures of UO_2^{2+} and its peroxo derivatives optimized at the B3LYP/B1 level in aqueous solution. The D_{2h} structure of the uranyl diperoxide was found to be a transition state structure.

dx.doi.org/10.1021/ic400652b | Inorg. Chem. 2013, 52, 5590−5602

Table 1. Energies and Characters of the MOs of the Dioxouranium(VI) Peroxides in Aqueous Solution Obtained at the B3LYP/B1 Level

$UO_2(O_2)$			$UO_2(O_2)_2^{2-}$			$UO_2(O_2)_3^{4-}$		
MO	energy (eV)	character	MO	energy (eV)	character	MO	energy (eV)	character
22	−11.32	$\sigma(O_2)$	26	−10.07	$\sigma(O_2)$	30	−9.19	$\sigma(O_2)$
23	−11.05	$\pi(O_2)/\pi$(d)	27	−9.77	$\sigma(O_2)$	31	−8.89	$\sigma(O_2)/\sigma$(d)
24	−10.77	$\pi(O_2)/\pi$(d)	28	−9.64	$\pi(O_2)/\sigma$(d)	32	−8.83	$\sigma(O_2)$
25	−9.84	σ(d)	29	−9.58	$\pi(O_2)/\pi$(d)	33	−8.82	$\sigma(O_2)$
26	−9.84	π(d)	30	−9.38	$\pi(O_2)/\pi$(d/f)	34	−8.50	$\pi(O_2)/\pi$(d)
27	−9.35	π(f)	31	−8.75	$\pi(O_2)/\pi$(f)	35	−8.50	$\pi(O_2)/\pi$(d)
28	−9.35	π(f)	32	−8.35	σ(d)	36	−8.13	$\pi(O_2)/\sigma$(f)
30	−8.11	σ(f)	33	−8.07	π(d/f)	37	−7.75	$\pi(O_2)/\pi$(d/f)
31	−7.40	$\sigma(U-O_2)$	34	−7.69	π(f)	38	−7.75	$\pi(O_2)/\pi$(d/f)
			35	−7.51	π(d)	39	−7.28	σ(d)
			36	−7.42	π(f)	40	−6.50	π(f)
			37	−6.57	σ(f)	41	−6.50	π(f)
			38	−6.03	$\sigma(U-O_2)$	42	−6.42	π(d)
						43	−6.42	π(d)
						44	−5.61	σ(f)
						45	−5.06	$\sigma(U-O_2)$

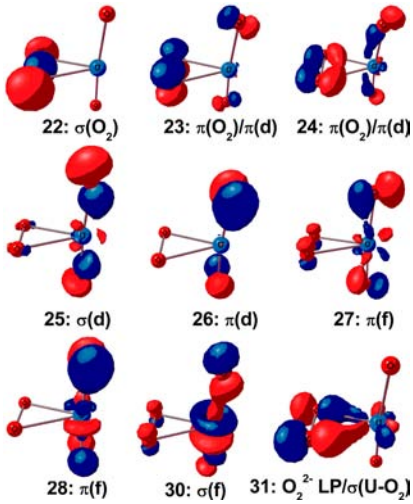

Figure 2. Molecular orbitals of $UO_2(O_2)$. The geometry of this complex was optimized with the PCM approach, and the B3LYP functional. LP represents lone pair for orbital 31.

moiety to more easily form peroxo species than its plutonyl counterpart.

The C_{2v} structure of $UO_2(O_2)_2^{2-}$, Figure 1, was calculated to be 3.1 kcal/mol more stable than its D_{2h} conformer in the aqueous phase. The energy difference in the gas phase was calculated as 1.2 kcal/mol. The D_{2h} structure is a transition state structure in both gaseous and aqueous media as it possesses imaginary frequencies of about 37i cm^{-1} and 76i cm^{-1}, respectively, in these media. These imaginary frequencies correspond to the equatorial bending of the O_2-U-O_2 group, Figure S1. The bent O_2-U-O_2 wing in the C_{2v} structure suggests a preference for circular polynuclear $(UO_2(O_2)_2)_n$-type species over the linear polymer species implied by the D_{2h} structure. The origins of the slightly greater stability of the C_{2v} structure in contrast to its D_{2h} conformer would be described at a later part of this section.

The calculated geometries of UO_2^{2+}, $UO_2(O_2)$, $UO_2(O_2)_2^{2-}$, and $UO_2(O_2)_3^{4-}$ obtained at the B3LYP/B1 level in aqueous solution are presented in Table 2. The calculated symmetric and asymmetric vibrational stretching modes of the uranyl groups in these complexes as well as the O_2 stretching and $U-O_2$ stretching modes of the peroxides are also presented in Table 2. The $O_{yl}-U-O_{yl}$ bond angle was calculated as 180.0°, 174.3°, 171.6°, and 180.0° in UO_2^{2+}, $UO_2(O_2)$, C_{2v}-$UO_2(O_2)_2^{2-}$, and $UO_2(O_2)_3^{4-}$, respectively. There is a sequential weakening of the $U-O_{yl}$, $U-O_{peroxo}$, $O-O_{peroxo}$ bonds as the number of coordinated peroxide ligands is increased. The

Table 2. Calculated Structural Properties and Vibrational Frequencies of UO_2^{2+} and Its Peroxo Derivatives Obtained at the B3LYP/B1 Level in Aqueous Solution

	bonds (Å)			vibrational frequencies (cm^{-1})				
				uranyl stretching			$U-O_2$ stretch	
	$U-O_{yl}$	$U-O_{peroxo}$	$O-O_{peroxo}$	asym	sym	O_2 stretch	sym	asym
UO_2^{2+}	1.748			1002	920			
$UO_2(O_2)$	1.810	2.177	1.442	854	789	936	472	464
$UO_2(O_2)_2^{2-}$								
C_{2v}	1.866	2.233/2.260	1.471	746	712	891/851	434/394	406/394
D_{2h}	1.861	2.259	1.467	755	713	891/856	393/392	397/370
$UO_2(O_2)_3^{4-}$	1.907	2.323	1.485	662	646	871/841/839	378/354/332	377/339/328
$UO_2(O_2)_3^{4-}$exptl	1.846[a]	2.303−2.324[a]						

[a]X-ray structure of $Li_4[UO_2(O_2)_3]_3 \cdot 10H_2O$, ref 15.

dx.doi.org/10.1021/ic400652b | Inorg. Chem. 2013, 52, 5590−5602

weaker U−O_{yl} bonds result in lower uranyl stretching vibrational frequencies. The uranyl stretching modes in $UO_2(O_2)_3^{4-}$ were calculated as 662 cm^{-1} for the asymmetric mode and 646 cm^{-1} for the symmetric mode. These are significantly lower than those obtained for the bare dication. To put this in perspective, the uranyl stretching modes in $UO_2(NO_3)_3^-$ and $UO_2(CO_3)_3^{4-}$, two complexes also possessing bidentate anionic ligands, were calculated as 870 and 929 cm^{-1} for the former and 775 and 811 cm^{-1} in the latter. In addition, the longer U−O_{peroxo} and O−O_{peroxo} bonds result in lower frequencies for the O_2 stretching and U−O_2 stretching vibrational modes, respectively. Similar elongations of the U−O_{yl} bonds have been observed in the uranyl hydroxide, $UO_2(OH)_n^{2-n}$,[58,59] and fluoride, $UO_2F_n^{2-n}$,[29] complexes. The simulated IR spectra of UO_2^{2+}, $UO_2(O_2)$, C_{2v}-$UO_2(O_2)_2^{2-}$, and $UO_2(O_2)_3^{4-}$ are shown in Figure 3. The vibrational modes

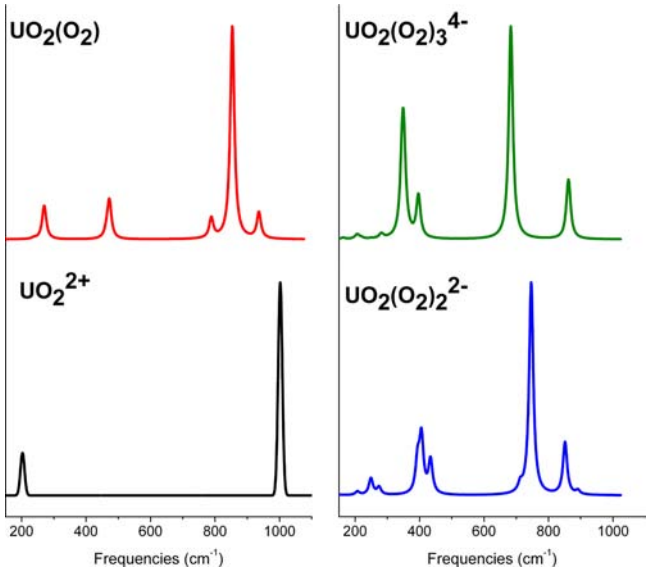

Figure 3. Simulated IR spectra of UO_2^{2+} and its peroxo derivatives obtained at the at the B3LYP/B1 level in aqueous solution.

associated with the stretching of the peroxo O−O bonds were found between 839 and 936 cm^{-1}, Table 2, gradually decreasing down the series and split across several frequencies in the diperoxo and triperoxo species. The calculated IR intensities of these peaks indicate that some of the O−O stretching should be observed in the Raman spectra of the peroxo complexes. The peak centered at around 470 cm^{-1} in the simulated IR spectra of $UO_2(O_2)$ and around 400 cm^{-1} in C_{2v}-$UO_2(O_2)_2^{2-}$ and $UO_2(O_2)_3^{4-}$, Figure 3, contains the U−O_{peroxo} stretching vibrations of which the symmetric mode has significantly higher IR intensities than the counterpart asymmetric mode. Similar to the case for the O−O stretching mode, the U−O_{peroxo} stretching vibrations are split into IR and Raman active modes in the higher peroxides. The U−O_{yl} bonds in $UO_2(O_2)_3^{4-}$ optimized with the PCM model are about 0.05 Å longer than those found in solid $Li_4[UO_2(O_2)_3]_3{\cdot}10H_2O$, Table 2.[15] It is noted that the crystal structure indicated interactions between the lithium-bound water molecules and the peroxide oxygen ligands. In implicit solvation models, like the PCM model employed here, the effect of a solvent is included with a statistically averaged solvent described by its dielectric constant, a macroscopic property. These models are not sufficient to describe the lithium-water and water-peroxo interactions in $Li_4[UO_2(O_2)_3]_3{\cdot}10H_2O$.

There are two types of U−O_{peroxo} bonds in the C_{2v} structure of $UO_2(O_2)_2^{2-}$, the proximal ones being about 0.03 Å longer than the distal ones, Figure 1. The $\sigma(O_2)$ character of MO-26 in C_{2v}-$UO_2(O_2)_2^{2-}$ is such that there is some overlap across the distal oxygen atoms of the two peroxo ligands, Figure 4. As this

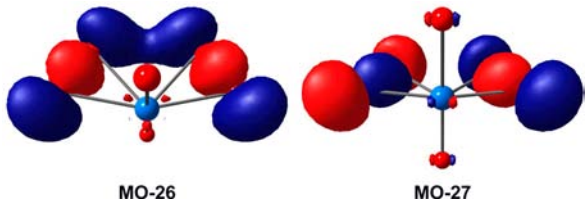

Figure 4. MO-26 and MO-27 of the C_{2v} structure of $UO_2(O_2)_2^{2-}$. The former is bonding with respect to the O−O′ distance between the distal oxygen atoms of the peroxo group while the latter is antibonding. The distal U−O bonds are about 0.03 Å shorter than the proximal ones.

overlap is prohibited in the D_{2h} structure, by virtue of the trans arrangement of the equatorial peroxo groups, it most likely contributes to the greater stability of the C_{2v} structure. Examination of the MO energy levels reveals that MO-26 (σ orbital bonding across the O−O′ distance, Figure 4) is about 6.92 kcal/mol below MO-27 (σ orbital antibonding across the O−O′ distance, Figure 4) in C_{2v}-$UO_2(O_2)_2^{2-}$. In contrast, the energy difference between these orbitals is 1.84 kcal/mol in D_{2h}-$UO_2(O_2)_2^{2-}$. This discrepancy indicates a stabilization of MO-26 in the C_{2v} structure. The difference in the relative energies of these orbitals (4.0 kcal/mol) is however not sufficient to fully explain the calculated greater stability of C_{2v}-$UO_2(O_2)_2^{2-}$ (3.1 kcal/mol in aqueous solution). As shown in Table S2 and Figure S4 of the Supporting Information, the 10 2p orbitals of $(O_2)_2^{2-}$ interact with the empty uranium 5f, 7s, and 6d orbitals to various extents in the C_{2v} and D_{2h} structures. Increased contributions from uranium atomic orbitals, generally found in D_{2h}-$UO_2(O_2)_2^{2-}$, result in destabilization of molecular orbitals with predominantly peroxo character. The converse is true for orbitals with mainly uranyl character.

The σ(U−O_2) orbitals of the U−O_{peroxo} bonds are formed by overlap of the uranium 5f orbitals and the in-plane π antibonding-type lone pair orbitals of the peroxo ligand, Figure 2. There is some U-6d contribution, 8%, to the σ(U−O_2) orbital in $UO_2(O_2)$. The U-6d orbitals however do not participate in the U−O_{peroxo} bonds of $UO_2(O_2)_2^{2-}$ and $UO_2(O_2)_3^{4-}$. These orbitals are most likely responsible for the covalent interactions between the peroxo and uranyl units. The out-of-plane peroxo π antibonding-type lone orbitals are found at higher energies.

The absolute ligand binding energies for $UO_2(O_2)$, C_{2v}-$UO_2(O_2)_2^{2-}$, and $UO_2(O_2)_3^{4-}$ were calculated as −121.5, −194.4, and −235.8 kcal/mol, respectively, at the B3LYP/B1 level in aqueous solution. These are the energies required to bind the peroxo ligands to the UO_2^{2+} and are equivalent to −121.5, −97.2, and −78.6 kcal/mol per peroxo group in these complexes, respectively. The binding energies were obtained from the calculated electronic energies of the species involved in the reaction: $UO_2^{2+}(aq) + nO_2^{2-}(aq) \rightarrow UO_2(O_2)_n^{2-2n}(aq)$. Although the absolute binding energies become larger for successive coordination of a peroxo ligand, the calculated binding energies relative to the $(n-1)$ species decrease down

dx.doi.org/10.1021/ic400652b | Inorg. Chem. 2013, 52, 5590−5602

Table 3. Calculated Structural Properties and Vibrational Frequencies (cm^{-1}) of $UO_2(H_2O)_5^{2+}$ and Its Peroxo Derivatives Obtained at the B3LYP/B1 Level in the Gas Phase and in Aqueous Solution

	bond lengths (Å)				uranyl stretching	
	$U-O_{yl}$	$U-O_{aquo}$	$U-O_{peroxo}$	$O-O_{peroxo}$	asym	sym
$UO_2(H_2O)_5^{2+}$						
gas phase	1.750	2.491			1026	937
solution	1.759	2.440−2.492			973	911
exptl	1.76[a]	2.41[a]			965[b]	870[b]
$UO_2(O_2)(H_2O)_4$						
gas phase	1.813	2.677/2.686	2.176	1.426	886	813
solution	1.815	2.644−2.666	2.195	1.440	840	789
$UO_2(O_2)(H_2O)_3$						
gas phase	1.814	2.593/2.600	2.162	1.429		
solution	1.814	2.549−2.557	2.186	1.445	843	791
$UO_2(O_2)(H_2O)_2$						
gas phase	1.808	2.571	2.141	1.435	893	820
solution	1.813	2.562/2.612	2.179	1.444	844	788
solution						
$UO_2(O_2)_2(H_2O)^{2-}$	1.866	2.727	2.240/2.264	1.471	739	704
cis-$UO_2(O_2)_2(H_2O)_2^{2-}$	1.862	2.725	2.251/2.275	1.469	749	718
trans-$UO_2(O_2)_2(H_2O)_2^{2-}$	1.865	2.645	2.267/2.279	1.466	741	709

[a]Reference 61. [b]References 62, .

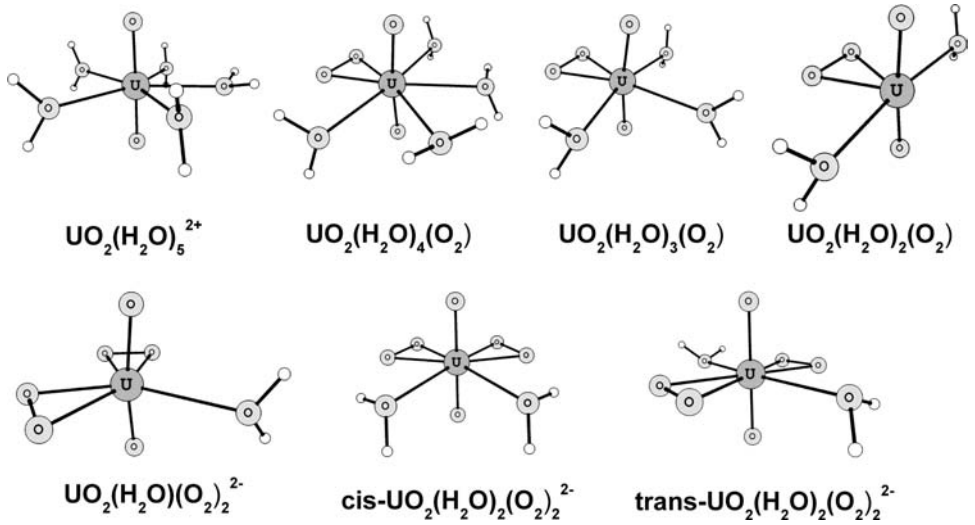

Figure 5. Structures of $UO_2(H_2O)_5^{2+}$ and its peroxo derivatives optimized at the B3LYP/B1 level in aqueous solution.

the series. A similar effect has been observed in our previous works on plutonyl hydroxides[58] and uranyl fluorides[29] as well as by other workers. For comparison, we also calculated the absolute ligand binding energies of $UO_2(OH)_4^{2-}$, $UO_2(NO_3)_3^{-}$, and $UO_2(CO_3)_3^{4-}$. These were calculated as −167.8, −55.4, and −148.0 kcal/mol, respectively, or −41.9, −18.5, −49.3 kcal/mol per ligand, respectively. The implication of this is that, for the UO_2L_n species (L = O_2^{2-}, OH, NO_3^{-}, or CO_3^{2-}), the uranyl group binds more strongly to the peroxide ligand than it does to the hydroxide, nitrate, and carbonate ligands. This is an indication of the binding between the uranyl and peroxide ligand, rather the formation energies of uranyl peroxo complexes. The formation of uranyl peroxides involves HO_2^{-} rather than O_2^{2-}. The trend in the calculated binding energies of the uranyl moiety with the equatorial ligands is in good agreement with recent findings.[60]

Uranyl Aquo Complexes. The uranyl chemistry in highly acidic solutions is dominated by the $UO_2(H_2O)_5^{2+}$ complex. The calculated bond lengths and vibrational frequencies of $UO_2(H_2O)_5^{2+}$ obtained in this work are presented in Table 3. Shamov et al. and several other workers have previously predicted the structure of this complex in the gas phase at the DFT level.[16,35,36,59] The calculated gas phase geometry of this complex obtained in this work is in good agreement with previous reports. Introduction of solvent effects with the continuum solvation model slightly weakens the $U-O_{yl}$ bonds by about 0.01 Å but strengthens the $U-OH_2$ interactions by about 0.05 Å. This is in accordance with previous computational work.[28,29,34−36] The use of the solvation model brings the calculated $U-O_{yl}$ and $U-OH_2$ bond-lengths to within 0.01 and 0.03 Å of the available aqueous phase extended X-ray absorption fine structure, EXAFS, data of Allen et al.[61] The calculated uranyl stretching vibrational frequencies are reduced by about 20−53 cm^{-1} in the solvent phase calculations. The experimental vibrational frequencies[62,63] of $UO_2(H_2O)_5^{2+}$ are

dx.doi.org/10.1021/ic400652b | Inorg. Chem. 2013, 52, 5590−5602

Table 4. Calculated Structural Properties and Vibrational Frequencies of $UO_2F_4^{2-}$ and Its Peroxo Derivatives Obtained at the B3LYP/B1 Level in Aqueous Solution

		bonds (Å)			vibrational frequencies (cm^{-1})				
					uranyl stretch			$U-O_2$ stretch	
	$U-O_{yl}$	$U-O_{peroxo}$	$O-O_{peroxo}$	U−F	asym	sym	O_2 stretch	sym	asym
$UO_2F_4^{2-}$	1.826			2.216	822	786			
exptl	1.800[a]			2.260[a]					
$UO_2F_3(O_2)^{3-}$	1.859	2.258	1.461	2.302	752	720	895	405	390
$UO_2F_2(O_2)^{2-}$	1.842	2.235	1.460	2.251	787	739	891	411	400
				2.260					
$UO_2F(O_2)_2^{3-}$	1.876	2.270−2.284	1.477	2.328	722	692	878/843	398	394
$UO_2F_2(O_2)_2^{4-}$									
cis	1.893	2.299−2.317	1.466	2.434	682	660	904/875	364/340	380/352
trans	1.893	2.309	1.465	2.423	687	664	904/880	352/345	360/343

[a]Reference 40.

within 41 cm^{-1} of the calculated values obtained using the PCM model.

The replacement of aquo ligands in $UO_2(H_2O)_5^{2+}$ by an equatorial peroxo group forms $UO_2(H_2O)_4(O_2)$, $UO_2(H_2O)_3(O_2)$, or $UO_2(H_2O)_2(O_2)$. This is interesting given that the chemical formulas of the minerals studtite and metastudtite are $UO_2(H_2O)_4(O_2)$ and $UO_2(H_2O)_2(O_2)$, respectively. The minerals however consist of polymeric chains bridged by peroxo units and coordinated water ligands.[64,65] The optimized structures for the aquo-peroxo complexes are presented in Figure 5. Starting from gas phase $UO_2(H_2O)_5^{2+}$ and HO_2^-, as shown in the reaction below, the formation of the aquo-peroxo complexes were calculated to be very exothermic in the gas phase, between −158.2 kcal/mol for $UO_2(H_2O)_2(O_2)$ and −187.1 kcal/mol for $UO_2(H_2O)_4(O_2)$.

$$UO_2(H_2O)_5^{2+} + HO_2^- \rightarrow UO_2(O_2)(H_2O)_n + (4-n)H_2O + H_3O^+$$

There is a drastic solvent effect, in excess of 150 kcal/mol, on these reactions. The magnitude of the solvent effect is not unusual and is a reflection of solvent screening of electrostatic charges, a phenomenon absent in the gaseous phase.[35,36,40,66,67] The formation of $UO_2(H_2O)_4(O_2)$ is still the most exothermic in the solution phase, about −13.7 kcal/mol compared to −6.7 and −8.7 kcal/mol for $UO_2(H_2O)_2(O_2)$ and $UO_2(H_2O)_3(O_2)$, respectively. This implies that the preferred equatorial coordination number of uranyl aquo-peroxo complex in the gas phase and in solution is 6, larger than that in the case of $UO_2(H_2O)_5^{2+}$.[35,36,68]

The $U-O_{yl}$ bond lengths in the aquo-peroxo complexes are centered at 1.814 Å with minimal changes both in solution and as the number of aquo ligands are increased from 2 to 4, Table 3. This represents a weakening of about 0.055 Å from $UO_2(H_2O)_5^{2+}$. The identical $U-O_{yl}$ bond lengths in these aquo-peroxo complexes are reflected in the similar calculated uranyl stretching vibrational frequencies, Table 3. The presence of the equatorial aquo ligands also has little influence on the length of the peroxo O−O bond. As a result the O−O stretching mode of $UO_2(O_2)$ calculated at 936 cm^{-1} in solution is retained in the aquo-peroxo complexes with very little change in its frequency. The $U-O_{peroxo}$ bonds become slightly longer from $UO_2(O_2)(H_2O)_2$ to $UO_2(O_2)(H_2O)_4$, weakening by 0.035 Å for the gaseous species and 0.016 Å in solution. The stretching modes associated with the $U-O_{peroxo}$ bonds are centered around 460−470 cm^{-1} just as in $UO_2(O_2)$, Figure 3. This is not surprising given that PCM calculations on bare $UO_2(O_2)$ species are essentially a crude model for the $UO_2(O_2)(H_2O)_n$ species with explicit first coordination aquo ligands. In contrast, the weakening of the $U-OH_2$ bonds after coordination of an equatorial peroxo ligand is significantly more pronounced, 0.08−0.20 Å in the gas phase and about 0.10 Å with the PCM model. The steric crowding between the aquo and peroxo ligands results in longer $U-OH_2$ bonds as the equatorial coordination number is increased.

It is reasonable to expect the formation of diperoxo species such as $UO_2(O_2)_2(H_2O)^{2-}$ or $UO_2(O_2)_2(H_2O)_2^{2-}$ at high peroxide concentrations. The calculated thermochemistry for the formation of these complexes in solution, via the reaction shown below, is however unfavorable. The reactions are endothermic for both $UO_2(O_2)_2(H_2O)^{2-}$, 22.7 kcal/mol, and $UO_2(O_2)_2(H_2O)_2^{2-}$, 18.1 kcal/mol. In a similar manner, the formation of the triperoxo complex, $UO_2(O_2)_3^{4-}$, from $UO_2(H_2O)_5^{2+}$, is endothermic in aqueous solution by 77.8 kcal/mol.

$$UO_2(H_2O)_5^{2+} + 2HO_2^- \rightarrow UO_2(O_2)_2(H_2O)_n^{2-} + (3-n)H_2O + 2H_3O^+$$

$$UO_2(H_2O)_5^{2+} + 3HO_2^- \rightarrow UO_2(O_2)_3^{4-} + 2H_2O + 3H_3O^+$$

Uranyl Fluoride Complexes. The structural properties of $UO_2F_4^{2-}$ as well as those of species formed by substitution of the fluoride ligands by peroxo groups are presented in Table 4. These geometrical features were obtained at the B3LYP/B1 level while employing the PCM solvation model. The optimized geometries for these complexes are presented in Figure 6. The calculated structural parameters of $UO_2F_4^{2-}$ are in good agreement with experimental data[67] and previous theoretical literature.[29,66,67] The $U-O_{yl}$ bonds were calculated to be about 0.03 Å longer than the experimental bond length of 1.800 Å. In contrast, the U−F bonds are about 0.04 Å shorter than the experimental value of 2.260 Å. The vibrational mode associated with the asymmetric stretching of the uranyl group was calculated as 822 cm^{-1} in good agreement with the experimental value. The experimental data on the structural properties of this complex were obtained by EXAFS, measurements in aqueous solution.[67]

dx.doi.org/10.1021/ic400652b | Inorg. Chem. 2013, 52, 5590−5602

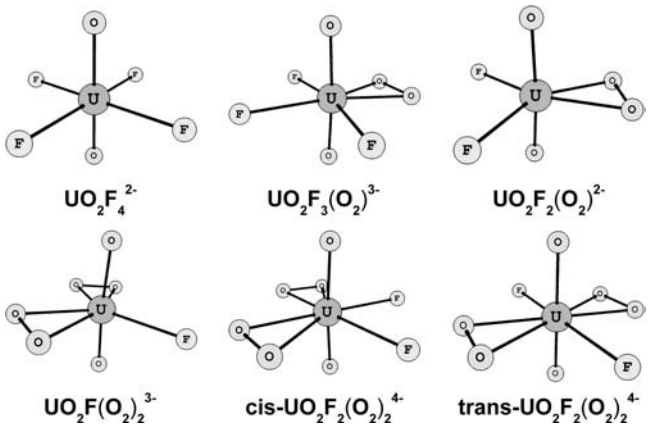

Figure 6. Structures of $UO_2F_4^{2-}$ and its peroxo derivatives optimized at the B3LYP/B1 level in aqueous solution.

Structurally, the U−O_{yl} bond lengths increase sequentially by about 0.02 Å down the $UO_2F_4^{2-}$, $UO_2F_2(O_2)^{2-}$, $UO_2F_3(O_2)^{3-}$, $UO_2F(O_2)_2^{3-}$, and $UO_2F_2(O_2)_2^{4-}$ series. The U−F and U−O_{peroxo} bonds also become progressively weaker down the series, Table 4. It is not entirely surprising that the U−O_{yl}, U−F, and U−O_{peroxo} bonds are longer in $UO_2F_3(O_2)^{3-}$ than in $UO_2F_2(O_2)^{2-}$, or in $UO_2F_2(O_2)_2^{4-}$ than in $UO_2F(O_2)_2^{3-}$. As previously noted, this trend toward weaker bonds as the number of equatorially coordinated anionic ligands is increased has been reported by various workers in uranyl hydroxides,[59,69] fluorides,[29] carbonates,[20] and nitrates.[20] Clark et al. suggested that the similar trend for the uranyl hydroxides was most likely due to competition between the axial oxo groups and the equatorial hydroxide ligands for the uranium 6d orbitals.[69] In our recent study of the plutonyl hydroxide complexes, $[PuO_2(H_2O)_{4-n}(OH)_n]^{2-n}$, we found that the Pu−OH bond is supported by both π-type and σ-type bond orbitals, with increasing Pu-6d contributions to these orbitals as the number of equatorial hydroxide ligands is increased and there is a simultaneous decrease in the Pu-6d contributions to the axial plutonyl π-orbitals.[58]

The binding energies of the fluoro groups to the uranyl peroxo cores, $UO_2(O_2)$ or $UO_2(O_2)_2^{2-}$, were calculated to be 23.9, 20.7, 13.6, and 5.2 kcal/mol per fluoro ligand in $UO_2F_2(O_2)^{2-}$, $UO_2F_3(O_2)^{3-}$, $UO_2F(O_2)_2^{3-}$, and $UO_2F_2(O_2)_2^{4-}$, respectively. This correlates well with the increasing U−F bond lengths down the series, Table 4. The weakening of the U−O_{yl} and U−O_{peroxo} bonds as the number of equatorial ligands in the ternary fluoro-peroxo complexes are increased results in lower wavenumbers for the O_{yl}−U-O_{yl} stretching modes as well as the U−O_{peroxo} stretching modes, Table 4. The symmetric and asymmetric uranyl stretching modes decrease from respectively 786 and 822 cm^{-1} in $UO_2F_4^{2-}$ to respectively 739 and 787 cm^{-1} in $UO_2F_2(O_2)^{2-}$. The coordination of an extra fluoride ligand in the equatorial region of $UO_2F_3(O_2)^{3-}$ further reduces the frequencies of these vibrational modes to 720 and 752 cm^{-1} respectively, Table 4. The symmetric and asymmetric U−O_{peroxo} stretching modes also decrease from 400 and 411 cm^{-1} in $UO_2F_2(O_2)^{2-}$ to 390 and 405 cm^{-1} in $UO_2F_3(O_2)^{3-}$. A similar pattern is also present in the fluoro-diperoxo and difluoro-diperoxo complexes, Table 4. We note that $UO_2F_2(O_2)^{2-}$ is topologically similar to the $UO_2(O_2)(CO_3)_2^{4-}$ ion. The asymmetric U−O_{peroxo} stretching mode of $UO_2F_2(O_2)^{2-}$ calculated at 400 cm^{-1} has a significantly lower IR intensity than the symmetric mode calculated at 411 cm^{-1}. The calculated peak at 400 cm^{-1} is in a way similar to the peak observed at 413.1 cm^{-1} in the Raman spectrum of $K_4[UO_2(O_2)(CO_3)_2].H_2O$.[12]

The reactions leading to the formation of the ternary fluoro-peroxo complexes from $UO_2(H_2O)_5^{2+}$ were studied at the B3LYP/B1 level in solution. These reactions take the form:

$$UO_2(H_2O)_5^{2+} + HO_2^- + (n)F^- \rightarrow UO_2(O_2)(F)_n^{-n} + 4H_2O + H_3O^+ \text{ (where } n = 2/3)$$

$$UO_2(H_2O)_5^{2+} + 2HO_2^- + (n)F^- \rightarrow UO_2(O_2)_2(F)_n^{-(n+2)} + 3H_2O + 2H_3O^+ \text{ (where } n = 1/2)$$

The calculated energies for these reactions are −44.9, −59.3, 10.9, and 14.1 kcal/mol for $UO_2F_2(O_2)^{2-}$, $UO_2F_3(O_2)^{3-}$, $UO_2F(O_2)_2^{3-}$, and $UO_2F_2(O_2)_2^{4-}$, respectively. First, the formation of the fluoro-diperoxo species in solution is endothermic, similar to the case with the aquo-diperoxo

Table 5. Calculated Structural Properties and Vibrational Frequencies of $UO_2(OH)_4^{2-}$ and Its Peroxo Derivatives Obtained at the B3LYP/B1 Level in Aqueous Solution

					vibrational frequencies (cm^{-1})				
	bonds (Å)				uranyl stretch			U−O_2 stretch	
	U−O_{yl}	U−O_{peroxo}	O−O_{peroxo}	U−OH	asym	sym	O_2 stretch	sym	asym
$UO_2(OH)_4^{2-}$	1.845			2.279	790	757			
expt	1.830[a]			2.265[a]	857[b]	784[b]			
$UO_2(OH)_3(O_2)^{3-}$	1.871	2.281	1.464	2.342−2.396	734	707	891	390	360
$UO_2(OH)_2(O_2)^{2-}$	1.851	2.247	1.468	2.286	774	731	872	419	401
$UO_2(OH)(O_2)_2^{3-}$	1.879	2.275	1.481	2.344	718	689	870	393	378
							836	384	357
		2.287							
				$UO_2(OH)_2(O_2)_2^{4-}$					
cis	1.897	2.314	1.471	2.472	682	664	894	370	341
		2.330					869	349	
trans	1.898	2.318	1.469	2.479	680	663	891	359	355
							872	336	330

[a]Reference 70. [b]References 71, 72.

dx.doi.org/10.1021/ic400652b | Inorg. Chem. 2013, 52, 5590−5602

complexes. On the other hand, the reactions leading to the formation of the monoperoxo complexes are significantly exothermic in solution.

Uranyl Hydroxide Complexes. The geometries of the hydroxo and hydroxo-peroxo analogues of the fluoro and fluoro-peroxo complexes discussed above were also optimized at the B3LYP/B1 level in aqueous solution. The calculated structural parameters and vibrational frequencies are presented in Table 5, and the structures are shown in Figure 7. Aqueous

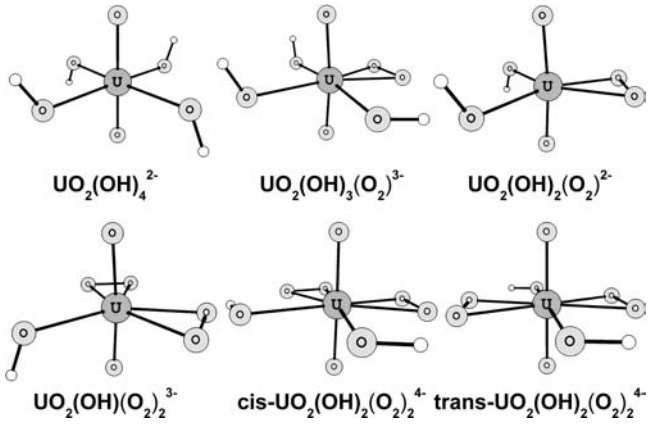

Figure 7. Structures of $UO_2(OH)_4^{2-}$ and its peroxo derivatives optimized at the B3LYP/B1 level in aqueous solution.

phase EXAFS measurement by Moll et al. provided U−O_{yl} and U−OH bonds lengths of 1.83 Å and 2.26 Å, respectively, for $UO_2(OH)_4^{2-}$.[70] The bond lengths obtained for these bonds from our theoretical calculations are within 0.02 Å of the EXAFS data, Table 5. The frequencies of the symmetric and asymmetric uranyl stretching vibrational modes in this complex were calculated to be 757 and 790 cm^{-1}, respectively, in solution. In the gas phase, the calculated frequencies of these vibrational modes are 756 and 826 cm^{-1}, respectively. The frequencies of these vibrations were found to be 784 and 857 cm^{-1} in aqueous phase measurement of the IR and Raman spectra of uranyl hydroxides by Quiles et al.[71,72] Clark et al. assigned the Raman peak at 796 cm^{-1} to the symmetric uranyl stretching mode in their characterization of a cobalt salt of the tetrahydroxide, $[Co(NH_3)_6]_2[UO_2(OH)_4]_3{\cdot}H_2O$.[69] Overall, it appears that the calculated vibrational frequencies obtained in the aqueous phase deviate from the experimental values by 30−70 cm^{-1}. Compared to the $UO_2F_4^{2-}$ complex, Table 4, the U−O_{yl} and U−ligand (U−OH/U−F) bonds are about 0.02 and 0.06 Å longer in the tetrahydroxo complex, Table 5. The origin of this bond weakening in the hydroxo complex is most likely the differences in the extents to which the 2p atomic orbitals of the equatorial ligands can compete with the oxo 2p orbitals for the U-6d orbitals. This is related to the π-donating abilities of the OH^- and F^- ligands. The longer U−O_{yl} bonds in $UO_2(OH)_4^{2-}$ are correlated with lower frequencies for the uranyl stretching modes in comparison to $UO_2F_4^{2-}$.

The reactions leading to the formation of $UO_2(OH)_2(O_2)^{2-}$, $UO_2(OH)_3(O_2)^{3-}$, $UO_2(OH)(O_2)_2^{3-}$, and $UO_2(OH)_2(O_2)_2^{4-}$ are similar to those written for the analogous fluoro-peroxo complexes:

$$UO_2(H_2O)_5^{2+} + HO_2^- + (n)OH^- \rightarrow UO_2(O_2)(OH)_n^{-n} + 4H_2O + H_3O^+ \text{ (where } n = 2/3)$$

$$UO_2(H_2O)_5^{2+} + 2HO_2^- + (n)OH^- \rightarrow UO_2(O_2)_2(OH)_n^{-(n+2)} + 3H_2O + 2H_3O^+ \text{ (where } n = 1/2)$$

The reaction energies for these are −57.7, −69.3, 6.3, and 8.1 kcal/mol for $UO_2(OH)_2(O_2)^{2-}$, $UO_2(OH)_3(O_2)^{3-}$, $UO_2(OH)(O_2)_2^{3-}$, and $UO_2(OH)_2(O_2)_2^{4-}$, respectively, in aqueous solution. The formation of the ternary hydroxo-peroxo complexes is significantly less exothermic than the formation of the analogous fluoro-peroxo complexes. However, like the aquo-diperoxo and fluoro-diperoxo complexes, the formation of the hydroxo-diperoxo species from HO_2^- was calculated to be endothermic in solution.

The optimized structures of the hydroxo-peroxo complexes are presented in Figure 7. The calculated U−O_{yl} bond lengths in these complexes, Table 5, are generally within 0.01 Å of those obtained for their fluoride counterparts, Table 4. As a result of this similarity in U−O_{yl} bond lengths, the calculated uranyl stretching vibrational frequencies of the hydroxo-peroxo species are generally within 20 cm^{-1} of those of the fluoro-peroxides. The U−O_{peroxo} bonds were calculated to be about 2.247 and 2.281 Å long in $UO_2(OH)_2(O_2)^{2-}$ and $UO_2(OH)_3(O_2)^{3-}$, respectively, Table 5. These can be compared to 2.235 and 2.258 Å for the difluoro and trifluoro monoperoxides, Table 4. The calculated U−O_{peroxo} stretching modes are found in the range 330−419 cm^{-1}, with the diperoxo species possessing two symmetric and two asymmetric U−O_{peroxo} stretching modes. This is similar to the case in the analogous fluoride complexes, Table 4, as well as in $UO_2(O_2)_2$, Table 2. Like the U−O_{yl} and U−O_{peroxo} bonds, the similarity of the O−O_{peroxo} bonds between the fluoro-peroxo and hydroxo-peroxo species results in similar calculated frequencies for the O_2 stretching vibrational modes.

The dihydro-diperoxo complex, $UO_2(OH)_2(O_2)_2^{4-}$, like its fluoride analogue has two conformers, a cis structure (C_{2v} or butterfly arrangement of the peroxo ligands) and a trans structure (D_{2h} arrangement of the peroxo ligands). The trans structure was found to be more stable than the cis conformer by 0.8 kcal/mol in aqueous solution. These structures are therefore isoenergetic, in contradiction to the case in $UO_2(O_2)_2^{2-}$, where the cis orientation of the peroxo ligands is favored by 3.1 kcal/mol. To explain the energy difference between the two conformers of $UO_2(O_2)_2^{2-}$, we examined the nature of the $\sigma(O_2)$-type orbitals and found some overlap across the two peroxo groups in the C_{2v} structure (see above and Figure 4). Examination of the low-energy valence orbitals of *cis*- and *trans*-$UO_2(OH)_2(O_2)_2^{4-}$ reveals MO-30 to be of predominantly σ(O−H) character, Figure 8. These orbitals

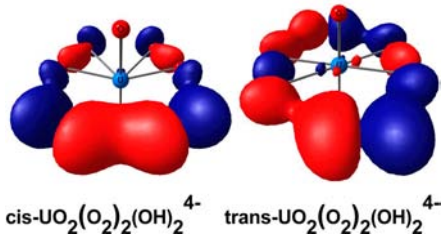

Figure 8. MO-30 of *cis*- and *trans*-$UO_2(O_2)_2(OH)_2^{4-}$. These orbitals are mostly of σ(O−H) character with substantial contributions from the O−O bonds of the peroxide.

dx.doi.org/10.1021/ic400652b | *Inorg. Chem.* 2013, 52, 5590−5602

Table 6. Calculated Structural Properties and Vibrational Frequencies (cm^{-1}) of $UO_2(CO_3)_3^{4-}$ and Its Peroxo Derivatives Obtained at the B3LYP/B1 Level in the Gas Phase and in Aqueous Solution

	bond lengths (Å)				uranyl stretching	
	U−O_{yl}	U−$O_{carbonate}$	U−O_{peroxo}	O−O_{peroxo}	asym	sym
$UO_2(CO_3)_3^{4-}$						
gas phase	1.822	2.535			839	773
solution	1.828	2.462			811	775
exptl	1.81[a]	2.44[a]			889[b]	813[b]
$UO_2(O_2)(CO_3)_2^{4-}$						
gas phase	1.848	2.636/2.641	2.272	1.461	796	730
solution	1.856	2.498/2.500	2.255	1.459	761	739
exptl	1.825−1.827[b]	2.429−2.473[b]	2.238−2.255[b]	1.469[b]		766.5[b]
$UO_2(O_2)_2(CO_3)^{4-}$						
solution	1.883	2.548	2.286/2.296	1.475	708	706

[a]Reference 75. [b]Reference 77.

Table 7. Calculated Structural Properties and Vibrational Frequencies (cm^{-1}) of $UO_2(NO_3)_3^{-}$ and Its Peroxo Derivatives Obtained at the B3LYP/B1 Level in the Gas Phase and in Aqueous Solution

	bond lengths (Å)				uranyl stretching	
	U−O_{yl}	U−$O_{nitrate}$	U−O_{peroxo}	O−O_{peroxo}	asym	sym
$UO_2(NO_3)_3^{-}$						
gas phase	1.776	2.503			957	875
solution	1.776	2.500			929	870
exptl	1.77[a]	2.48−2.50[a]			943−967[b]	875−886[b]
$UO_2(O_2)(NO_3)_2^{2-}$						
gas phase	1.821	2.662/2.709	2.187	1.446	858	787
solution	1.822	2.589/2.619	2.198	1.451	824	777
$UO_2(O_2)_2(NO_3)^{3-}$						
solution	1.869	2.714	2.252/2.264	1.473	735	703

[a]Reference 76. [b]Reference 78.

however have significant $\sigma(O_2)$-type contributions. From an analysis of the orbital compositions, the $\sigma(O_2)$-type contributions to MO-30 are larger for the trans conformer of $UO_2(OH)_2(O_2)_2^{4-}$. This compensates for the lacking overlap between the two peroxo units, Figure 4, and is responsible for the isoenergetic nature of the two conformers. Similar arguments are applicable to the fluoride analogues. As for $UO_2F_2(O_2)_2^{4-}$, attempts to optimize the structure of $UO_2(OH)_2(O_2)_2^{4-}$ in the gas phase failed as the molecule fragmented into its component anionic pieces. Zehnder et al. have recently characterized $Na_6[UO_2(O_2)_2(OH)_2]$-$(OH)_2{\cdot}14H_2O$ using single crystal X-ray diffraction techniques.[73] They found that the $UO_2(OH)_2(O_2)_2^{4-}$ anion in $Na_6[UO_2(O_2)_2(OH)_2](OH)_2{\cdot}14H_2O$ has two trans peroxo groups and two trans hydroxo ligands. Compared to $Na_6[UO_2(O_2)_2(OH)_2](OH)_2{\cdot}14H_2O$ (U−O_{yl}, 1.862 Å; U−O_{peroxo}, 2.289/2.308 Å; U−O_{OH}, 2.388 Å; and O−O_{peroxo}, 1.480 Å), the structural parameters of *trans*-$UO_2(OH)_2(O_2)_2^{4-}$ that we optimized in solution appears to be sufficiently close (within 0.03 Å), Table 5. The only exceptions are the U−OH bonds which are about 0.09 Å longer than those found in the sodium salt. To confirm the stabilization of the $UO_2F_2(O_2)_2^{4-}$ and $UO_2(OH)_2(O_2)_2^{4-}$ species in solution, we checked that the errors in the total polarization charges obtained for the PCM calculations, a reflection of the portion of the density lying outside the cavity, were in all cases less than 0.05. We also examined the volume of the cavity and the spatial extent of the virtual molecular orbitals in the complexes.

Uranyl Carbonates and Nitrates. The formation of $UO_2(O_2)(CO_3)_2^{4-}$ and $UO_2(O_2)_2(CO_3)^{4-}$, from $UO_2(H_2O)_5^{2+}$ by addition of HO_2^- and the carbonate ion, follow the reaction

$$UO_2(H_2O)_5^{2+} + (n)HO_2^- + (3-n)CO_3^{2-} \rightarrow UO_2(O_2)_n(CO_3)_{3-n}^{4-} + (3-n)H_2O + (n)H_3O^+$$

The reaction energies were calculated as −59.8 and 6.3 kcal/mol for $UO_2(O_2)(CO_3)_2^{4-}$ and $UO_2(O_2)_2(CO_3)^{4-}$, respectively, at the B3LYP/B1 level in aqueous solvent. For the analogous nitrate species, $UO_2(O_2)(NO_3)_2^{2-}$ and $UO_2(O_2)_2(NO_3)^{3-}$, the reaction energies are −16.7 and 20.4 kcal/mol, respectively. These reaction energies suggest that the diperoxo species should not be observed in solution. In a contemporaneous paper, Grenthe et al. have reported the speciation of the uranyl-peroxide-carbonate system using a combination of potentiometric and NMR measurements.[74] $UO_2(O_2)(CO_3)_2^{4-}$ and $UO_2(O_2)(CO_3)^{2-}$ were the only species with one uranyl group identified in their experiments. Most of the other species observed in their data contained two uranyl groups. The absence of $UO_2(O_2)_2(CO_3)^{4-}$, in the experimental speciation data of Grenthe et al., even at high H_2O_2 concentrations, is consistent with the calculated reaction energies obtained in this work. The reaction energies for the formation of the nitrate-peroxo complexes are higher than those of their carbonate counterparts, in line with the fact that NO_3^- is a much weaker ligand for uranyl than CO_3^{2-}.

Structurally, the U−O_{yl} bonds are shorter in the nitrate complexes than in the counterpart carbonate complexes, Tables 6 and 7. Comparison of the nitrato-peroxo and carbonato-

dx.doi.org/10.1021/ic400652b | Inorg. Chem. 2013, 52, 5590−5602

peroxo complexes to the fluoro-peroxo, Table 4, the hydroxo-peroxo, Table 5, and bare peroxo, Table 2, complexes indicates that the U−O_{yl} bonds become increasingly weaker as the interactions between the uranyl and equatorial ligands become stronger. The calculated U−O_{yl} bond lengths in $UO_2(CO_3)_3^{4-}$ (see Figure 9) and $UO_2(NO_3)_3^-$ obtained in either the gaseous

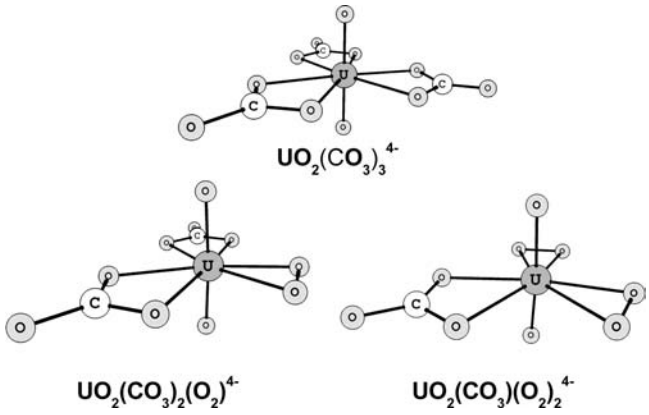

Figure 9. Structures of $UO_2(CO_3)_3^{4-}$ and its peroxo derivatives optimized at the B3LYP/B1 level in aqueous solution. The analogous nitrate complexes possess similar structural frameworks.

phase or in solution are about 0.01−0.02 Å longer than the experimental values. It should be noted that the experimental values were obtained from solid state X-ray or neutron diffraction studies of alkali metal salts of $UO_2(CO_3)_3^{4-}$ and $UO_2(NO_3)_3^-$.[75,76] Assuming that this discrepancy between the calculated and experimental U−O_{yl} bond lengths observed in the tricarbonate and trinitrate complexes can be transferred to the peroxo complexes brings the calculated U−O_{yl} bond lengths in $UO_2(O_2)(CO_3)_2^{4-}$ into agreement with the experimental value of 1.825−1.827 Å obtained from the crystallographic data of $K_4[UO_2(O_2)(CO_3)_2]\cdot H_2O$.[12]

The U−$O_{nitrate}$ bond length in $UO_2(NO_3)_3^-$ was calculated as 2.503 and 2.500 Å in the gas and aqueous phases, respectively, Table 7. In contrast, the solvent effect on the U−$O_{carbonate}$ bond length is significantly higher, Table 6. Similar to the U−O_{yl} bonds, the U−$O_{nitrate}$ and U−$O_{carbonate}$ bonds become weaker on coordination of a peroxo group. In the calculations carried out in aqueous solution, the U−$O_{carbonate}$ bonds increase from 2.462 Å in the tricarbonate complex to 2.548 Å in the diperoxo-monocarbonate complex. The U−$O_{nitrate}$ bonds in the diperoxo-mononitrate complex are about 2.714 Å long. The U−$O_{carbonate}$ bonds distal to the peroxo group in $UO_2(O_2)(CO_3)_2^{4-}$ are slightly shorter (by 0.005 and 0.002 Å in the gaseous and aqueous phases respectively) than those proximal to the peroxo group, Table 6. Similarly, the distal U−$O_{nitrate}$ bonds in $UO_2(O_2)(NO_3)_2^{2-}$ are shorter than their proximal counterparts by 0.047 and 0.030 Å in the gas and aqueous phases, respectively, Table 7. The trend in the U−O_{peroxo} bond lengths in the ternary peroxo-nitrate and peroxo-carbonate complexes is similar to those observed for the U−O_{yl} and U−$O_{carbonate/nitrate}$ bonds.

In the calculations with the PCM solvation model, the bond between the oxygen atoms of the peroxide ligands was calculated to be about 1.442 Å long in $UO_2(O_2)_2^{2-}$ and 1.471 Å long in $UO_2(O_2)_2^{2-}$, Table 2. This bond is slightly longer (about 1.460 Å) in the monoperoxo-fluoro complexes, Table 4, as well as in the monoperoxo-carbonate complex (1.459 Å) and in the monoperoxo-nitrate complex (1.451 Å). The calculated O−O bond length in $UO_2(O_2)(CO_3)_2^{4-}$ is in good agreement with the experimental value of 1.469 Å obtained Goff et al.[12] in their work on $K_4[UO_2(O_2)(CO_3)_2]\cdot 1H_2O$.

The calculated vibrational frequencies of the peroxo-carbonate and peroxo-nitrate complexes are also presented in Tables 6 and 7, respectively. The modes associated with asymmetric and symmetric stretching of the uranyl group in $UO_2(CO_3)_3^{4-}$ were calculated as 839 cm^{-1} and 773 cm^{-1}, respectively, in the gas phase. This calculated symmetric stretching frequency is within the range obtained previously by Schlosser et al.[32] and de Jong et al.[20] The inclusion of the solvent effects with the PCM model has little effect on the symmetric stretching frequency but reduces the asymmetric stretching mode by about 28 cm^{-1} in comparison to the gas phase. The calculated IR active asymmetric uranyl stretching frequency deviates from the experimental value by about 71 cm^{-1} in the aqueous phase while its symmetric counterpart has an error of about 31 cm^{-1}.[77] In contrast, the agreement between the B3LYP/B1 model and the experimental vibrational frequencies is improved for $UO_2(NO_3)_3^-$, Table 7. The symmetric stretching mode was calculated to have a frequency of 870 cm^{-1} in good agreement with solid state Raman spectroscopic measurements (876−886 cm^{-1}) of uranyl nitrate salts.[78] The gas phase calculations provided a value of 875 cm^{-1} for this vibrational mode, little change from the calculations with the PCM model and in good agreement with the solid-state crystal measurements. The frequencies of the uranyl asymmetric stretching vibrational mode were found to be 943.1 and 967.2 cm^{-1} in the potassium and ammonium crystalline salts from solid-state IR measurements.[78] The calculated frequencies of this vibrational mode in the gaseous and aqueous phases are within 14−38 cm^{-1} of these experimental values, Table 7.

For the peroxo derivative of $UO_2(CO_3)_3^{4-}$ and $UO_2(NO_3)_3^-$, the calculated frequencies of the asymmetric and symmetric uranyl stretching modes decrease by 30−55 cm^{-1} for each carbonate substitution in the peroxo-carbonate series, Table 6, and about 70−100 cm^{-1} for each nitrate substitution in the peroxo-nitrate series, Table 7. For the monoperoxo carbonate complex, the calculated frequencies of the symmetric uranyl stretching mode, 739 cm^{-1} in solution and 730 cm^{-1} in the gas phase, are in agreement with the experimental value of 766.5 cm^{-1} obtained during Raman spectral measurements of $K_4[UO_2(O_2)(CO_3)_2]\cdot H_2O$.[12] Another notable vibrational mode in $UO_2(O_2)(CO_3)_2^{4-}$ is the C−O stretch, calculated at 1054 cm^{-1} in good agreement with the experimental value of 1053 cm^{-1} in the potassium hydrate complex.[12] The vibrational mode associated with the C−O_3 bending of both carbonate groups (asymmetric out of plane deformations) is Raman active and was calculated to have frequencies of, respectively, 847 and 842 cm^{-1} in the gaseous and aqueous phase calculations on $UO_2(O_2)(CO_3)_2^{4-}$. The same mode is also Raman active in the calculated spectra of $UO_2(CO_3)_3^{4-}$, 849 and 842 cm^{-1} in the gaseous and aqueous phases, respectively. Peaks corresponding to this vibrational mode were observed between 849 and 879 cm^{-1} in the combined Raman and infrared (IR) work of Anderson et al.[79] on $K_4[UO_2(CO_3)_3]$. In addition, de Jong et al.[20] obtained a value of 845 cm^{-1} in their theoretical study of uranyl carbonate using the local density approximation (LDA) with diffuse basis sets. We note that the peak at 841.7 cm^{-1} in the Raman spectrum of $K_4[UO_2(O_2)(CO_3)_2]\cdot 2.5H_2O$ was however labeled as the O−O symmetric stretching mode by

dx.doi.org/10.1021/ic400652b | Inorg. Chem. 2013, 52, 5590−5602

Table 8. Calculated Mayer Bond Orders in Various Uranyl Complexes and Their Peroxo Derivatives Obtained at the B3LYP/B2 Level Using Structures Optimized at the B3LYP/B1 Level

	$U-O_{yl}$	$U-O_{peroxo}$	$O-O_{peroxo}$	$U-X_{ligand}$		$U-O_{yl}$	$U-O_{peroxo}$	$O-O_{peroxo}$	$U-X_{ligand}$
UO_2^{2+}	2.53				halides				
$UO_2(O_2)$	2.42	1.23	1.01		$UO_2F_4^{2-}$	2.29			1.02
C_{2v}-$UO_2(O_2)_2^{2-}$	2.31	1.05/1.08	0.98		$UO_2(O_2)F_2^{2-}$	2.31	1.07	0.98	1.00
$UO_2(O_2)_3^{4-}$	2.25	1.03	0.98		$UO_2(O_2)F_3^{3-}$	2.26	1.05	0.99	0.96
aquo					$UO_2(O_2)_2F^{3-}$	2.27	1.02	0.97	0.95
$UO_2(H_2O)_5^{2+}$	2.43			0.46−0.49	$UO_2(O_2)_2F_2^{4-}$	2.26	1.04	0.99	0.94
$UO_2(O_2)(H_2O)_2$	2.40	1.20		0.34	hydroxides				
$UO_2(O_2)(H_2O)_3$	2.39	1.18	1.00	0.34	$UO_2(OH)_4^{2-}$	2.32			1.07
$UO_2(O_2)(H_2O)_4$	2.39	1.17	1.01	0.30	$UO_2(O_2)(OH)_2^{2-}$	2.32	1.08	0.98	1.06
$UO_2(O_2)_2(H_2O)^{2-}$	2.31	1.06	0.98	0.24	$UO_2(O_2)(OH)_3^{3-}$	2.29	1.06	0.98	1.00−1.03
$UO_2(O_2)_2(H_2O)_2^{2-}$					$UO_2(O_2)_2(OH)^{3-}$	2.28	1.02	0.97	1.02
trans	2.30	1.00/1.04	0.98	0.25	$UO_2(O_2)_2(OH)_2^{4-}$	2.26	1.04	0.99	0.99
cis	2.32	1.00/1.04	0.97	0.24	nitrates				
carbonates					$UO_2(NO_3)_3^-$	2.38			0.48
$UO_2(CO_3)_3^{4-}$	2.31			0.68	$UO_2(O_2)(NO_3)_2^{2-}$	2.35	1.13	1.00	0.36
$UO_2(O_2)(CO_3)_2^{4-}$	2.29	1.05	0.99	0.64	$UO_2(O_2)_2(NO_3)^{3-}$	2.28	1.02−1.04	0.98	0.28
$UO_2(O_2)_2(CO_3)^{4-}$	2.26	1.00−1.02	0.98	0.61					

Goff et al.[12] The frequency of the O−O symmetric stretching mode in $UO_2(O_2)(CO_3)_2^{4-}$ was however calculated to be at 890 and 894 cm^{-1} in the gas phase and in solution, respectively. This particular mode was calculated to be at 944 cm^{-1} in PCM calculations on H_2O_2 in contrast to the experimental value of 875 cm^{-1}. It is most likely the case that the assignment of the strong peak at 841.7 cm^{-1} to the O−O symmetric stretching mode by Goff et al. is correct given the seemingly large error in the calculated frequencies for this mode. The symmetric and asymmetric stretching of the $U-O_{peroxo}$ bonds in $UO_2(O_2)(CO_3)_2^{4-}$ were calculated, respectively, as 383 and 375 cm^{-1} in the gas phase and 394 and 387 cm^{-1} in solution. The asymmetric stretching modes, which were calculated to possess low IR intensities, might account for the peak at 431.0 cm^{-1} in the Raman spectrum of $K_4[UO_2(O_2)(CO_3)_2]\cdot 2.5H_2O$. The simulated IR spectra of uranyl tricarbonate and trinitrate as well as those of their monoperoxo derivatives are shown in Figure S2.

Bond Orders in the Uranyl and Uranyl Peroxo Complexes. The population-based Mayer bond orders obtained for all the bonds in the uranyl and uranyl peroxo complexes studied in this work are collected in Table 8. The calculated bond orders for the $U-O_{yl}$ bonds in UO_2^{2+}, $UO_2(H_2O)_5^{2+}$, $UO_2(NO_3)_3^-$, $UO_2(OH)_4^{2-}$, $UO_2(CO_3)_3^{4-}$, and $UO_2F_4^{2-}$ decrease down the series. The orders for these bonds range from 2.53 in the bare dication to 2.29 in the tetrafluoro complex. These values indicate that the $U-O_{yl}$ bonds possess significant triple bond character with the presence of equatorial ligands diminishing the triple bond nature. From the degree of perturbation of the $U-O_{yl}$ bonds, as seen in the bond order reduction, it appears that the aquo and nitrate ligands have the weakest covalent interaction with the uranyl groups. This is supported by the $U-O_{water}$ and $U-O_{nitrate}$ bond orders of 0.48 and 0.46−0.49, respectively, that are far smaller than the $U-O_{carbonate}$, $U-F_{fluoride}$, and $U-O_{hydroxide}$ bond orders, respectively, of 0.68, 1.02, and 1.07, Table 8. It is most likely that a competition between the $U-O_{yl}$ and $U-X_{ligand}$ bonds for uranium 6d atomic contributions result in the weakening of the $U-O_{yl}$ bonds with increasing π-donating abilities of the equatorial ligand. This correlates with the fact that the U−OH bonds have the highest bond order of the equatorial $U-X_{ligand}$ bonds. As previously mentioned, it has recently been shown that there is an increase in the actinide 6d contributions to the An−OH bonds and a simultaneous decrease in the An 6d contributions to the $An-O_{yl}$ bonds on progressing down the AnO_2^{2+} to $AnO_2(OH)_4^{2-}$ (An = U, Np and Pu) series.[58] Going forward, we are interested in using more comprehensive charge and orbital decomposition schemes to examine the interplay between covalent and electrostatic interactions in determining the strength of the equatorial bonds in actinide complexes.

For the uranyl peroxo complexes, $UO_2(O_2)$, $UO_2(O_2)_2^{2-}$, and $UO_2(O_2)_3^{4-}$, the calculated bond orders for the $U-O_{yl}$ bonds decrease from 2.42 to 2.25, reminiscent of the case for the fluoro, hydroxo, aquo, nitrate, and carbonate complexes. The $U-O_{peroxo}$ bond orders also decrease from 1.23 in the monoperoxo species to 1.03 in the triperoxo complex. The inclusion of other ligands in the equatorial region of $UO_2(O_2)$ leads to a slight decrease in the $U-O_{yl}$ bond orders. A similar case is observed for the $U-O_{peroxo}$ bonds, with the calculated bond order depending on the binding strength of the other equatorial ligands. For the strongly binding carbonate, hydroxo, and fluoro equatorial ligands, the $U-O_{peroxo}$ bond orders are about 1.05−1.08 while for the weakly binding aquo and nitrate ligands, the $U-O_{peroxo}$ bond orders are about 1.13−1.20. The bond orders for the O−O bonds of the peroxide ligand remain within the range 0.97−1.01 regardless of the number of peroxo groups in the complex as well as the nature of the other equatorial ligands.

The very strong affinity of the peroxo group for the uranyl moiety as well as its interaction with the uranium 5f and 6d orbitals, as shown in Figure 2 and Table 1, suggest that it could stabilize the bent cis-uranyl unit.[80−83] The relative energies of the cis- and trans-uranyl peroxo complexes are examined in the Supporting Information.

■ CONCLUSIONS

The structural and electronic properties of various uranyl peroxo complexes have been examined using scalar relativistic DFT calculations. The aqueous-phase structures of the peroxo complexes were modeled with the PCM solvation model. The

dx.doi.org/10.1021/ic400652b | Inorg. Chem. 2013, 52, 5590−5602

reaction energies for the formation of the uranyl peroxo complexes from their parent uranyl complexes, the relative stabilities of the various structures of the peroxo complexes, as well as the role of the equatorial peroxo group on the trans−cis transformation (Supporting Information) of the uranyl moiety were all examined in the gaseous and aqueous phases.

The affinity of the peroxo ligand for the uranyl group far exceeds that of the F^-, OH^-, CO_3^{2-}, NO_3^-, and H_2O ligands. The reactions leading to the formation of the various uranyl-monoperoxo complexes from $UO_2(H_2O)_5^{2+}$ and HO_2^- were calculated to be significantly exothermic in both the gaseous and aqueous phases. As a result, the U(VI) and peroxo concentrations, both kinetic factors, are the major factors in experimentally identifying the mononuclear uranyl-peroxo species studied in this work. It should be noted however that the formation of the diperoxo $UO_2(O_2)_2X_2^{4-}$/$UO_2(O_2)_2X^{4/3-}$ species from $UO_2(H_2O)_5^{2+}$ and HO_2^- were all calculated to be endothermic in aqueous medium. This implies that the monouranyl-diperoxo complexes of the aquo, fluoro, hydroxo, carbonate, and nitrate ligands would be absent in solution in very good agreement with recent experimental data. On the other hand, attempts to optimize the geometries of these complexes in the gas phase failed as they decomposed to the component anions. This indicates the crucial roles of counterions in the crystallization of the $UO_2(O_2)_2X_2^{4-}$/$UO_2(O_2)_2X^{4/3-}$ species.

Examination of the electronic structures of the uranyl-peroxo complexes reveals that the $U-O_{peroxo}$ bond is formed by overlap between U(VI) 5f orbitals and in-plane π antibonding-type lone pair orbitals of the peroxo ligand. The σ and π bonding orbitals between the oxygen atoms of the peroxo ligands are more stable than the orbitals of the uranyl moiety. There is however significant $\pi-\pi$ mixing between the orbitals of the peroxo ligand and the π(d) orbitals of the uranyl. The importance of $\pi(O_2)-\pi$(f) mixing is higher for the diperoxo and triperoxo complexes as the inclusion of the second and third peroxo ligands further stabilizes the uranyl π(f) orbitals. For $UO_2(O_2)_2^{2-}$, a cis arrangement of the peroxo groups was calculated to be more stable than the D_{2h} structure which features a trans arrangement of the equatorial peroxo groups. The origin of this difference was found to be the presence of an overlap between the distal oxygen atoms of the two peroxo groups in the $\sigma(O_2)$ orbitals. In contrast for the $UO_2(O_2)_2X_2^{4-}$ (for X = F^- and OH^-) species, the structures with cis and trans peroxo groups are iso-energetic as the $\sigma(O_2)$ orbitals now contain overlap with the σ(O−H) and F_{2p} orbitals.

The trends in the structures of the uranyl-peroxo complexes with the F^-, OH^-, CO_3^{2-}, NO_3^-, and H_2O ligands are similar to those previously observed in other uranyl complexes. Inclusion of the peroxo ligand weakens the $U-O_{yl}$ bonds resulting in sequentially decreasing uranyl vibrational frequencies. The O−O bond of the peroxo complexes is mostly centered at 1.455−1.480 Å, and as such the O−O stretching vibrational mode is found between 840 and 940 cm^{-1}. The calculated bond orders of the O−O bonds were found to be between 0.96 and 1.02, in good correlation with the little influence on the O−O bond lengths by the type and nature of equatorial ligands. The $U-O_{peroxo}$ bond-lengths are somewhat more sensitive to the type and number of coordinated anionic ligands. The $U-O_{peroxo}$ stretching modes were calculated to be between 330 and 419 cm^{-1}, with the symmetric mode being IR active and the asymmetric mode, Raman active.

■ ASSOCIATED CONTENT

Supporting Information

Full citation for ref 42. Figures S1−S4. Table S1 detailing gas phase optimized structures of uranyl and uranyl peroxo species. Cartesian coordinates of the optimized structures of the title complexes. Table S2 detailing molecular orbitals of the C_{2v} and D_{2h} versions of $[UO_2(O_2)_2]^{2-}$. Table S3 and accompanying discussion detailing the effect of the peroxo ligand on the stability of the cis/bent uranyl group. This material is available free of charge via the Internet at http://pubs.acs.org.

■ AUTHOR INFORMATION

Corresponding Author

*E-mail: samuel.odoh@pnnl.gov (S.O.O.); schrecke@cc.umanitoba.ca (G.S.).

Present Address

[†]Environmental Molecular Sciences Laboratory, Pacific Northwest National Laboratory, P.O. Box 999, Richland, Washington 99352, United States.

Notes

The authors declare no competing financial interest.

■ ACKNOWLEDGMENTS

The authors thank Dr. Grigory Shamov for helpful discussions. S.O.O. gratefully thanks the estate of Ernst and Ingrid Buck, the University of Manitoba, and the Provincial Government of Manitoba, Canada, for their financial support. G.S. acknowledges financial support from the Natural Sciences and Engineering Research Council of Canada (NSERC).

■ REFERENCES

(1) Sigmon, G. E.; Ling, J.; Unruh, D. K.; Moore-Shay, L.; Ward, M.; Weaver, B.; Burns, P. C. *J. Am. Chem. Soc.* **2009**, *131*, 16648.
(2) Clarens, F.; de Pablo, J.; Casas, I.; Gimenez, J.; Rovira, M.; Merino, J.; Cera, E.; Bruno, J.; Quinones, J.; Martinez-Esparza, A. *J. Nucl. Mater.* **2005**, *345*, 225.
(3) Gimenez, J.; Clarens, F.; Casas, I.; Rovira, M.; de Pablo, J.; Bruno, J. *J. Nucl. Mater.* **2005**, *345*, 232.
(4) Kubatko, K. A.; Forbes, T. Z.; Klingensmith, A. L.; Burns, P. C. *Inorg. Chem.* **2007**, *46*, 3657.
(5) Ling, J.; Wallace, C. M.; Szymanowski, J. E. S.; Burns, P. C. *Angew. Chem., Int. Ed.* **2010**, *49*, 7271.
(6) Sigmon, G. E.; Weaver, B.; Kubatko, K. A.; Burns, P. C. *Inorg. Chem.* **2009**, *48*, 10907.
(7) Unruh, D. K.; Burtner, A.; Pressprich, L.; Sigmon, G. E.; Burns, P. C. *Dalton Trans.* **2010**, *39*, 5807.
(8) Corbel, C.; Sattonnay, G.; Guilbert, S.; Garrido, F.; Barthe, M. F.; Jegou, C. *J. Nucl. Mater.* **2006**, *348*, 1.
(9) Armstrong, C. R.; Nyman, M.; Shvareva, T.; Sigmon, G. E.; Burns, P. C.; Navrotsky, A. *Proc. Natl. Acad. Sci. U.S.A.* **2012**, *109*, 1874.
(10) Miro, P.; Pierrefixe, S.; Gicquel, M.; Gil, A.; Bo, C. *J. Am. Chem. Soc.* **2010**, *132*, 17787.
(11) Vlaisavljevich, B.; Gagliardi, L.; Burns, P. C. *J. Am. Chem. Soc.* **2010**, *132*, 14503.
(12) Goff, G. S.; Brodnax, L. F.; Cisneros, M. R.; Peper, S. M.; Field, S. E.; Scoft, B. L.; Runde, W. H. *Inorg. Chem.* **2008**, *47*, 1984.
(13) Meca, S.; Martinez-Torrents, A.; Marti, V.; Gimenez, J.; Casas, I.; de Pablo, J. *Dalton Trans.* **2011**, *40*, 7976.
(14) Zanonato, P. L.; Di Bernardo, P.; Grenthe, I. *Dalton Trans.* **2012**, *41*, 3380.
(15) Nyman, M.; Rodriguez, M. A.; Campana, C. F. *Inorg. Chem.* **2010**, *49*, 7748.
(16) Austin, J. P.; Sundararajan, M.; Vincent, M. A.; Hillier, I. H. *Dalton Trans.* **2009**, 5902.

(17) Batista, E. R.; Martin, R. L.; Hay, P. J. *J. Chem. Phys.* **2004**, *121*, 11104.
(18) Bühl, M.; Sieffert, N.; Chaumont, A.; Wipff, G. *Inorg. Chem.* **2011**, *50*, 299.
(19) Bühl, M.; Sieffert, N.; Chaumont, A.; Wipff, G. *Inorg. Chem.* **2012**, *51*, 1943.
(20) de Jong, W. A.; Apra, E.; Windus, T. L.; Nichols, J. A.; Harrison, R. J.; Gutowski, K. E.; Dixon, D. A. *J. Phys. Chem. A* **2005**, *109*, 11568.
(21) de Jong, W. A.; Harrison, R. J.; Nichols, J. A.; Dixon, D. A. *Theor. Chem. Acc.* **2001**, *107*, 22.
(22) Garcia-Hernandez, M.; Lauterbach, C.; Krüger, S.; Matveev, A.; Rösch, N. *J. Comput. Chem.* **2002**, *23*, 834.
(23) Han, Y. K. *J. Comput. Chem.* **2001**, *22*, 2010.
(24) Han, Y. K.; Hirao, K. *J. Chem. Phys.* **2000**, *113*, 7345.
(25) Hay, P. J.; Martin, R. L. *J. Chem. Phys.* **1998**, *109*, 3875.
(26) Kovacs, A.; Konings, R. J. M. *THEOCHEM* **2004**, *684*, 35.
(27) Odoh, S. O.; Schreckenbach, G. *J. Phys. Chem. A* **2010**, *114*, 1957.
(28) Odoh, S. O.; Schreckenbach, G. *J. Phys. Chem. A* **2011**, *115*, 14110.
(29) Odoh, S. O.; Walker, S. M.; Meier, M.; Stetefeld, J.; Schreckenbach, G. *Inorg. Chem.* **2011**, *50*, 3141.
(30) Pereira, C. C. L.; Marsden, C. J.; Marcalo, J.; Gibson, J. K. *Phys. Chem. Chem. Phys.* **2011**, *13*, 12940.
(31) Privalov, T.; Schimmelpfennig, B.; Wahlgren, U.; Grenthe, I. *J. Phys. Chem. A* **2002**, *106*, 11277.
(32) Schlosser, F.; Moskaleva, L. V.; Kremleva, A.; Krüger, S.; Rösch, N. *Dalton Trans.* **2010**, *39*, 5705.
(33) Schreckenbach, G.; Hay, P. J.; Martin, R. L. *J. Comput. Chem.* **1999**, *20*, 70.
(34) Schreckenbach, G.; Shamov, G. A. *Acc. Chem. Res.* **2010**, *43*, 19.
(35) Shamov, G. A.; Schreckenbach, G. *J. Phys. Chem. A* **2005**, *109*, 10961.
(36) Shamov, G. A.; Schreckenbach, G. *J. Phys. Chem. A* **2006**, *110*, 12072.
(37) Shamov, G. A.; Schreckenbach, G.; Vo, T. N. *Chem.—Eur. J.* **2007**, *13*, 4932.
(38) Straka, M.; Kaupp, M. *Chem. Phys.* **2005**, *311*, 45.
(39) Tsushima, S.; Uchida, Y.; Reich, T. *Chem. Phys. Lett.* **2002**, *357*, 73.
(40) Vallet, V.; Macak, P.; Wahlgren, U.; Grenthe, I. *Theor. Chem. Acc.* **2006**, *115*, 145.
(41) Vukovic, S.; Watson, L. A.; Kang, S. O.; Custelcean, R.; Hay, B. P. *Inorg. Chem.* **2012**, *51*, 3855.
(42) Frisch, M. J.; et al. *Gaussian 03, Revision C.02*; 2004.
(43) Miertus, S.; Scrocco, E.; Tomasi, J. *Chem. Phys.* **1981**, *55*, 117.
(44) Küchle, W.; Dolg, M.; Stoll, H.; Preuss, H. *Mol. Phys.* **1991**, *74*, 1245.
(45) Küchle, W.; Dolg, M.; Stoll, H.; Preuss, H. *J. Chem. Phys.* **1994**, *100*, 7535.
(46) Lim, I. S.; Stoll, H.; Schwerdtfeger, P. *J. Chem. Phys.* **2006**, 124.
(47) Becke, A. D. *J. Chem. Phys.* **1993**, *98*, 5648.
(48) Lee, C. T.; Yang, W. T.; Parr, R. G. *Phys. Rev. B.* **1988**, *37*, 785.
(49) Stephens, P. J.; Devlin, F. J.; Chabalowski, C. F.; Frisch, M. J. *J. Phys. Chem.* **1994**, *98*, 11623.
(50) Laikov, D. N.; Ustynyuk, Y. A. *Russ. Chem. B+* **2005**, *54*, 820.
(51) Laikov, D. N. *Chem. Phys. Lett.* **2005**, *416*, 116.
(52) Denning, R. G. *Struct. Bonding (Berlin)* **1992**, *79*, 215.
(53) Denning, R. G. *J. Phys. Chem. A* **2007**, *111*, 4125.
(54) Denning, R. G.; Foster, D. N. P.; Snellgrove, T. R.; Woodwark, D. R. *Mol. Phys.* **1979**, *37*, 1089.
(55) Denning, R. G.; Green, J. C.; Hutchings, T. E.; Dallera, C.; Tagliaferri, A.; Giarda, K.; Brookes, N. B.; Braicovich, L. *J. Chem. Phys.* **2002**, *117*, 8008.
(56) Denning, R. G.; Snellgrove, T. R.; Woodwark, D. R. *Mol. Phys.* **1976**, *32*, 419.
(57) Denning, R. G.; Snellgrove, T. R.; Woodwark, D. R. *Mol. Phys.* **1979**, *37*, 1109.
(58) Odoh, S. O.; Reyes, J. A.; Schreckenbach, G. *Inorg. Chem.* **2013** , submitted.
(59) Ingram, K. I. M.; Haller, L. J. L.; Kaltsoyannis, N. *Dalton Trans.* **2006**, 2403.
(60) Vallet, V.; Wahlgren, U.; Grenthe, I. *J. Phys. Chem. A* **2012**, *116*, 12373.
(61) Allen, P. G.; Bucher, J. J.; Shuh, D. K.; Edelstein, N. M.; Reich, T. *Inorg. Chem.* **1997**, *36*, 4676.
(62) Jones, L. H.; Penneman, R. A. *J. Chem. Phys.* **1953**, *21*, 542.
(63) Toth, L. M.; Begun, G. M. *J. Phys. Chem.* **1981**, *85*, 547.
(64) Walenta, K. *Am. Mineral.* **1974**, *59*, 166.
(65) Weck, P. F.; Kim, E.; Jove-Colon, C. F.; Sassani, D. C. *Dalton Trans.* **2012**, *41*, 9748.
(66) Garcia-Hernandez, M.; Willnauer, C.; Krüger, S.; Moskaleva, L. V.; Rosch, N. *Inorg. Chem.* **2006**, *45*, 1356.
(67) Vallet, V.; Wahlgren, U.; Schimmelpfennig, B.; Moll, H.; Szabo, Z.; Grenthe, I. *Inorg. Chem.* **2001**, *40*, 3516.
(68) Tsushima, S.; Yang, T. X.; Suzuki, A. *Chem. Phys. Lett.* **2001**, *334*, 365.
(69) Clark, D. L.; Conradson, S. D.; Donohoe, R. J.; Keogh, D. W.; Morris, D. E.; Palmer, P. D.; Rogers, R. D.; Tait, C. D. *Inorg. Chem.* **1999**, *38*, 1456.
(70) Moll, H.; Reich, T.; Szabo, Z. *Radiochim. Acta* **2000**, *88*, 411.
(71) Quiles, F.; Burneau, A. *Vib. Spectrosc.* **2000**, *23*, 231.
(72) Quiles, F.; Chinh, N. T.; Carteret, C.; Humbert, B. *Inorg. Chem.* **2011**, *50*, 2811.
(73) Zehnder, R. A.; Batista, E. R.; Scott, B. L.; Peper, S. M.; Goff, G. S.; Runde, W. H. *Radiochim. Acta* **2008**, *96*, 575.
(74) Zanonato, P. L.; Di Bernardo, P.; Szabo, Z.; Grenthe, I. *Dalton Trans.* **2012**, *41*, 11635.
(75) Amayri, S.; Reich, T.; Arnold, T.; Geipel, G.; Bernhard, G. *J. Solid State Chem.* **2005**, *178*, 567.
(76) Barclay, G. A.; Sabine, T. M.; Taylor, J. C. *Acta Crystallogr.* **1965**, *19*, 205.
(77) Allen, P. G.; Bucher, J. J.; Clark, D. L.; Edelstein, N. M.; Ekberg, S. A.; Gohdes, J. W.; Hudson, E. A.; Kaltsoyannis, N.; Lukens, W. W.; Neu, M. P.; Palmer, P. D.; Reich, T.; Shuh, D. K.; Tait, C. D.; Zwick, B. D. *Inorg. Chem.* **1995**, *34*, 4797.
(78) McGlynn, S. P.; Neely, W. C.; Smith, J. K. *J. Chem. Phys.* **1961**, *35*, 105.
(79) Anderson, A.; Chieh, C.; Irish, D. E.; Tong, J. P. K. *Can. J. Chem.* **1980**, *58*, 1651.
(80) Hratchian, H. P.; Sonnenberg, J. L.; Hay, P. J.; Martin, R. L.; Bursten, B. E.; Schlegel, H. B. *J. Phys. Chem. A* **2005**, *109*, 8579.
(81) Schreckenbach, G.; Hay, P. J.; Martin, R. L. *Inorg. Chem.* **1998**, *37*, 4442.
(82) Vaughn, A. E.; Barnes, C. L.; Duval, P. B. *Angew. Chem., Int. Ed.* **2007**, *46*, 6622.
(83) Villiers, C.; Thuery, P.; Ephritikhine, M. *Angew. Chem., Int. Ed.* **2008**, *47*, 5892.